PROCEEDINGS OF SCIENCE

The Time Evolution of the Surface Detector of the Pierre Auger Observatory

Orazio Zapparrata[a,*] **for the Pierre Auger Collaboration**[b]

[a] *Université Libre de Bruxelles, Brussels, IIHE, Belgium*

[b] *Observatorio Pierre Auger, Av. San Martín Norte 304, 5613 Malargüe, Argentina*

Full author list: https://www.auger.org/archive/authors_icrc_2023.html

E-mail: spokespersons@auger.org

The surface detector array of the Pierre Auger Observatory, consisting of 1660 water Cherenkov tanks, has been in operation for nearly 20 years. During this long period of data acquisition, ageing effects in the detector response have been observed. The temporal evolution of the signals recorded by the surface detector is mostly compensated by continuous calibration with atmospheric muons; however, effects persist in the signal rise time and in high-level data analysis using neural networks. We have implemented a detailed description of the time evolution of the detector response and of the uptimes of individual stations in GEANT4-based detector simulations. These new simulations reproduce the observed time dependencies in the data. Using air-shower simulations that take into account the evolution of individual stations, we show that the reconstructed energy is stable at the sub-percent level, and its resolution is affected by less than 5% in 15 years. For a few specific stations, the collected light produced by muons has decreased to the point where it is difficult to distinguish it from the electromagnetic background in the calibration histograms. The upgrade of the Observatory with scintillator detectors mitigates this problem: by requiring a coincidence between the water-Cherenkov and scintillator detectors, we can enhance the muon relative contribution to the calibration histogram. We present the impact and performance of this coincidence calibration method.

38th International Cosmic Ray Conference (ICRC2023)
26 July - 3 August, 2023
Nagoya, Japan

*Speaker

PoS(ICRC2023)266

1. Introduction

The Pierre Auger Observatory is the largest experiment ever built to detect air showers and to infer the properties of primary cosmic rays with energies above 10^{17} eV. The Surface Detector (SD), one of its main components, comprises 1660 water-Cherenkov detectors (WCD) spread over an area of 3000 km^2. These tanks have a height of 1.2 m and a diameter of 3.6 m, and are filled with 12 t of ultra-pure water contained in a liner bag with internal walls covered with a reflective material called Tyvek^{TM}. The WCDs have been operating in the field for almost 20 years, showing decreased recorded signals over time. This long-term effect is known as the ageing of the detector, which can impact high-level variables, such as risetime and the mean number of triggered stations. Even the reconstruction of the primary cosmic rays could be affected, since the shower energy estimator is obtained from the fit of the lateral distribution of the calibrated signals recorded by the stations [1]. Understanding these effects can help improve systematics and verify the robustness of the calibration procedure.

The calibration of the SD has been designed to be robust, reliable, and automatically self-performed on each tank on the field every minute [2]. This procedure, along with continuous monitoring of the stations' conditions, ensured the acquisition of quality data over the years by exploiting the uniform flux of secondary particles produced by low-energy showers. In this way, a uniform calibration and trigger conditions for the full array is attained, using, in particular, atmospheric muons passing through the tanks at a rate of $\approx$ 3 kHz. The Cherenkov light produced by relativistic charged particles traversing the water, often multiply-reflected by the internal walls, is collected by each of its three photomultipliers (PMTs) looking downwards. The amplitude and the charge of signals generated by atmospheric particles are used to build the so-called calibration histograms for charge and peak. An example of charge calibration histograms for two different years can be seen in Fig. 1 (left). In these histograms, atmospheric muons generate the hump on the right, while the hump on the left is due to $e^{\pm}$ and γ. Since atmospheric muons produce a distinctive response in the detector, the signal produced by vertical muons (VEM) passing through a station is used to calibrate each SD station independently, ensuring a common reference between them. The VEM is obtained for each station by scaling the hump in the charge histogram produced by omnidirectional muons (Q_{VEM}) with a conversion factor obtained from a dedicated muon telescope on a reference WCD at the beginning of the operation of the Observatory, and more recently, using an RPC hodoscope [3].

The Observatory has also undergone a recent and almost complete upgrade [4], called AugerPrime, in which additional detectors have been added to enhance the sensitivity to the different components of extensive air showers. In particular, a Surface Scintillator Detector (SSD) has been placed on top of each WCD. This upgrade opened an unforeseen possibility to improve the calibration method further and ensure the acquisition of high-quality data in the next coming years of the Observatory operations, which are planned to continue at least until 2035.

2. Long-term evolution of the Surface Detector

The constant evaluation and measurement of several parameters at the station level during calibration reveals changes in the detector's response to secondary particles over the years. This effect can be noticed in Fig. 1 where two charge histograms from different years show a shift in

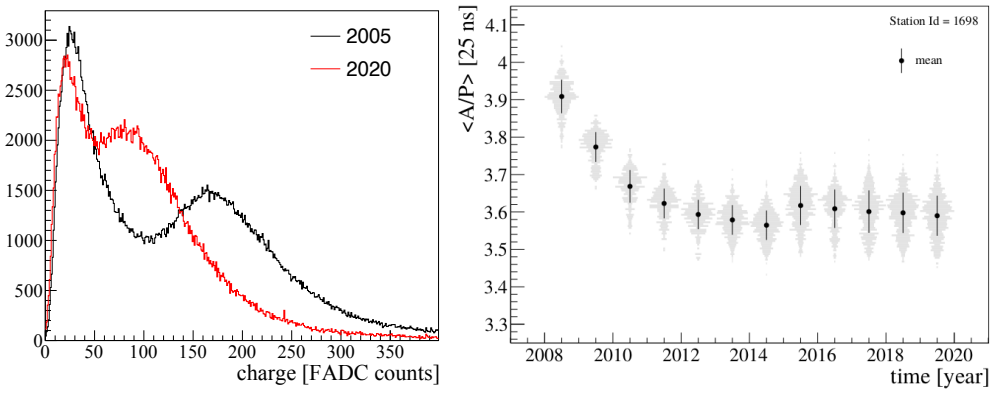

Figure 1: Left: Example of charge calibration histograms for a station (Maya Evelyn) exhibiting strong ageing effects. Year 2005 (black line) and 2020 (red line), PMT 3. Right: Area over Peak for station Denisa Maria as a function of time, PMTs combined. Uncertainties are defined as the RMS of the distributions.

the position of the muon hump towards lower values in the more recent year, causing the muonic component to merge with the electromagnetic background, making it more difficult to find the position of the muon hump. The ageing effects of the SD are visible in the slow decrease of the "Area over Peak ratio", denoted by A/P, where A is the average total charge and P is the average maximum value of pulses from vertical muons. The A/P is used to monitor the changes in the station response over time. The reduction of A/P reflects a decrease in the light collection efficiency and can be induced by a change in the optical properties of the detector, such as liner reflectivity and water transparency. The A/P decreases over time for all PMTs, with almost 20% of them having had a reduction of the A/P of more than 15% over 14 years [5]. An example of A/P evolution over time for a selected station is shown in Fig. 1 (right). Around 165 events per year are selected when applying quality cuts to remove outliers and a clear decrease from 3.9 ± 0.02[25 ns] to 3.6 ± 0.02[25 ns] between 2008 and 2014 is visible before stabilizing[1] around 3.6 ± 0.03[25 ns]. Pulses from vertical muons can be selected amongst the signals produced by secondary particles from low-energy showers by requiring an integrated charge of $(1.0 \pm 0.1) \cdot Q_{VEM}$. The sum of these signals, called the *pulse shape histogram*, shows a sharp rise followed by an exponential decrease caused by the multiple reflections of Cherenkov photons inside the tank. The light-decay constant of these histograms, denoted as τ, is related to the propagation and collection efficiency of Cherenkov photons, probing, in particular, changes in the reflectivity of the internal walls. Indeed, a decrease in the liner reflectivity will cause fewer photons to reach the PMTs, producing steeper signals. The difference in the signal shape over time can be observed in Fig. 2 (left), where histograms are normalized to their peak and obtained as the mean between the maximum and minimum PMTs signals for each specific event. An exponential fit is performed to extract τ, as follows:

$$f(x) = A \cdot e^{-\frac{x}{\tau}} \tag{1}$$

The lower edge of the fit has been chosen to avoid the first reflections or the direct light that reaches the PMTs, thus only the central part of the signal is considered where we expect to have a cloud of

[1]The jump observed in 2015 is caused by the freezing of water inside the tanks.

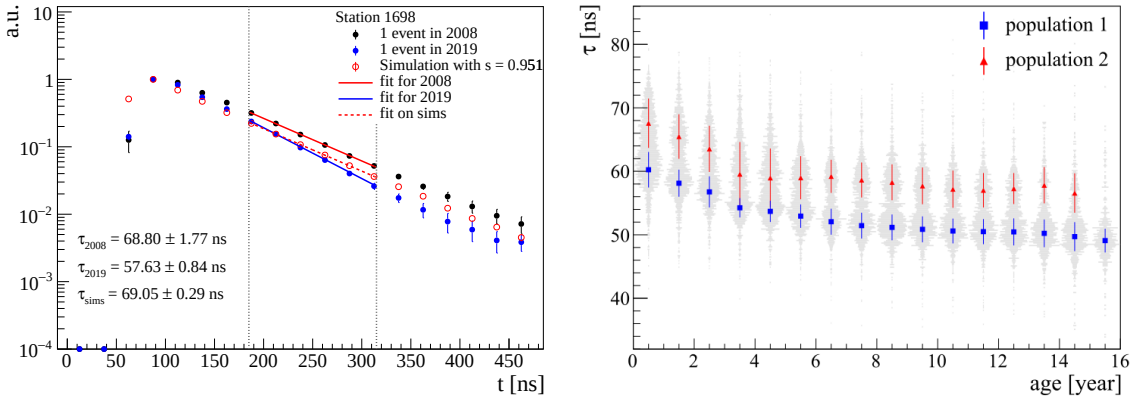

Figure 2: Left: Example of shape calibration histograms for station Denisa Maria for 2008 (black) and 2019 (blue) and a simulation with internal reflectivity of 0.95 (best match in 2008). Error bars represent the spread between the PMTs. Exponential fits are shown as lines. Right: τ evolution as a function of station age for the full array. The uncertainties represent the standard deviation of the fitted Gaussians and the gray shadows show the distribution of the mean τ of the stations in a specific year.

randomized photons that went through multiple reflections inside the tank. In this way, the effect of the overall internal reflectivity is enhanced. The upper edge is chosen to avoid possible biases from a low number of photoelectrons. It can be noticed how the shape of the signals has changed in 11 years, with a decrease of τ of ≈11 ns. The evolution of τ as function of time after deployment (denoted here as "age" of the tank) for all the stations, Fig. 2 (right), shows a bimodal distribution, with one of the two populations not being present in the last years, indicating that the second population was deployed later. The mean τ for each year's distribution for the two populations is obtained by fitting a sum of two Gaussians. Even if the two populations show different values of τ, their decrease over time is compatible. The population with the highest values (red points) exhibits a decrease of τ from 68 ns to 57 ns in 15 years, while for the other population τ starts at 60 ns and drops to 50 ns in the same time interval.

In this work, we assume that changes in the reflectivity of the liner are the main cause for the observed effect, however, we cannot distinguish it from a probable change in the photon absorption in the water. To reproduce the observed ageing in the signal, a model of the evolution over time of this reflectivity is needed. To simulate the calibration histograms, we used simulations of low-energy air showers (mostly protons, 88%, and ^{4}He, 10%) with a median energy between 10 GeV and 100 GeV, and we injected secondary particles reaching the ground in detector simulations. The majority of these secondary particles are high energy muons around 1 GeV, while γ and $e^{\pm}$ contributions dominate the low energy range, around 100 MeV. Different station conditions were simulated by varying the liner reflectivity (s). 200 million simulation instances of secondary particles were injected in station simulations with more than 1000 different values of s. Using these simulations, we modeled the ageing by matching τ obtained by fitting the shape histograms from data collected by the SD and simulations. To quantify the differences between measured and simulated shape histograms, we defined a quadratic distance based on τ, as follows:

$$d_\tau^2 = \frac{(\tau_{\text{data}} - \tau_{\text{sims}})^2}{\delta\tau_{\text{data}}^2 + \delta\tau_{\text{sims}}^2} \tag{2}$$

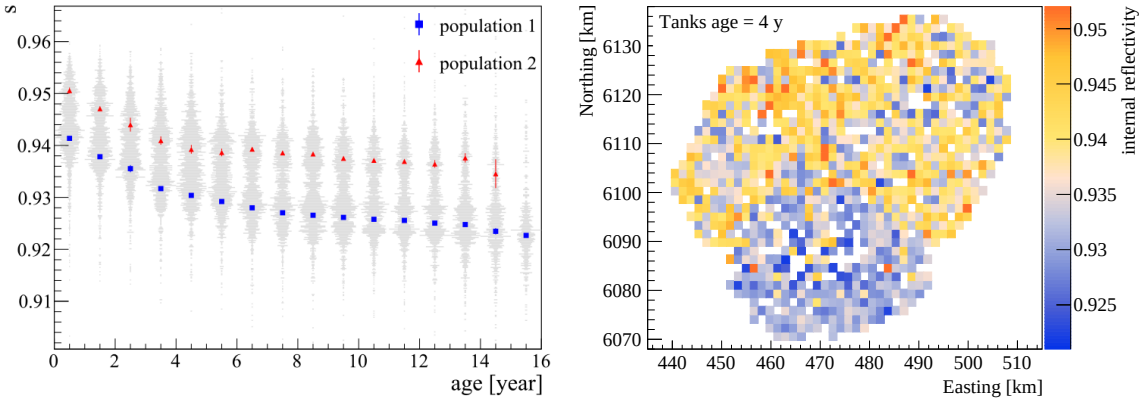

Figure 3: Left: s evolution as a function of the station age, for the full array. Two different populations are observed. Right: Spatial distribution of the internal reflectivity values at the station age of 4 years.

The best match between data and simulations is obtained by finding the minimum of d^2_τ as a function of τ for each event in the dataset. In this way, the liner reflectivity best reproducing the measured τ was found, as shown with the simulated shape histogram (open red symbols) in Fig. 2 (left). In this example, the muon pulses in 2008 could be well described by assuming a reflectivity of 0.95. This method was applied to all the stations of the array. A general decrease of s over time can be seen in Fig. 3 (left). A bimodal distribution is present, with a decrease of reflectivity, on average, of 1.7% in 15 years, describing well the decrease of the light-decay with a difference in s between the two populations of $\approx$ 1%. The mean s for the two populations at each age is obtained by fitting a sum of two Gaussians, and the errors on the mean are used for its uncertainties for a given age. The spatial distribution of s over the array, Fig. 3 (right), shows that stations with lower values of reflectivity (population 1) are mostly located in the southern area of the array, while the second population appears more in the northern part. This pattern correlates with the unfolding of the deployment, with the southern part of the array having been deployed first.

To assess the impact on the reconstruction due to a signal loss, the ageing model was then implemented in the Offline [6] framework, producing a time-dependent simulation of the SD, changing the properties of each tank based on the corresponding liner reflectivity obtained from the model at the time of the simulated event. Each station's acquisition status, including the deployment roll-out, has been included in simulations thanks to the information obtained by the T2 triggers received by the Central Data Acquisition System (CDAS) [7]. A full library of reconstructed showers has been produced using, as input, simulated air showers produced with `CORSIKA` 7.7420 [8] and EPOS-LHC [9] as hadronic models for four different primaries (p, He, O, Fe). The energy range considered was $18.5 < \log_{10}(E/eV) < 20.2$, with a uniform angular distribution in $\cos^2\theta$ for $\theta < 65°$ and four different atmospheres. The total number of `CORSIKA` showers amounted to almost 67.000. Each air-shower has been thrown multiple times at random positions over the array, and all the events, uniformly distributed between 2005 and 2020, were reconstructed with two different detector configurations: a fixed reflectivity for all the stations (*ideal* mode) and a setup including the time evolution of the SD (*ageing SD* mode). The official SD reconstruction and the related quality cuts were applied [1], resulting in $\approx$ 1 million reconstructed showers. Simulated events were

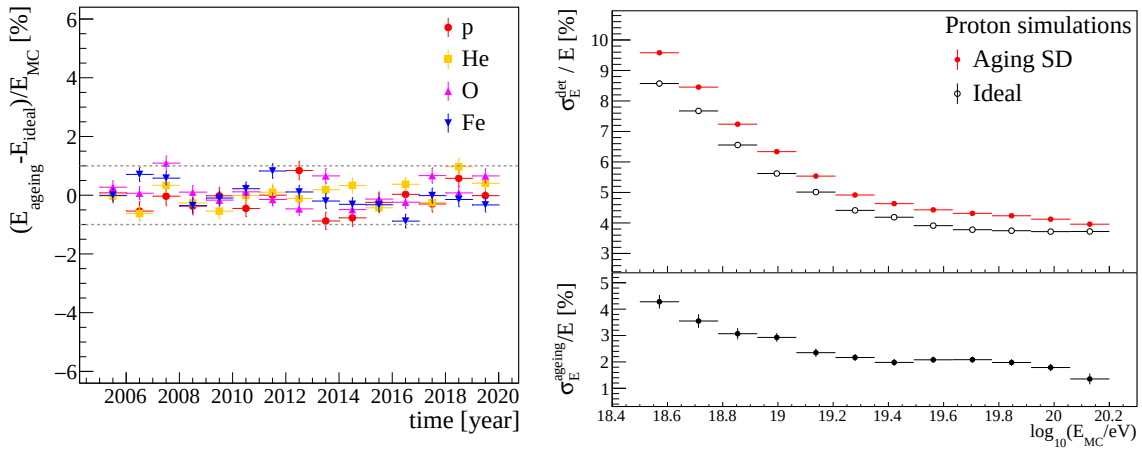

Figure 4: Left: Change of the energy bias over time for the two different simulation configurations of the array: an ideal SD and a SD with a time-dependent behavior. Right: SD resolution (top panel) and resolution due to the ageing (bottom panel) as a function of the primary energy for the two modes.

weighted following the measured energy spectrum [10] since the energy bias in the reconstruction depends on the primary particle's energy. The difference in the energy bias between the two modes as a function of time is shown in Fig. 4 (left): even in the case of a reduction of the signal due to the ageing, it can be noticed that the reconstructed energy remains stable over the years, with variations at the sub-percent level. These results prove the robustness of the continuous calibration using atmospheric muons employed in Auger.

The energy resolution, however, has been found to be marginally affected. To study the effect of the time evolution of the detector in more detail, the detector energy resolution, $\sigma_E^{\rm det}$, is obtained from the reconstructed events generated at different times from the same primary particle that has been thrown several times in the array. This way, the only effects are due to the detector and the core location, and shower-to-shower fluctuations are avoided. The $\sigma_E^{\rm det}$ dependency on the primary energy (E_{MC}), proton in this case, can be seen in the right upper plot of Fig. 4 for both *ideal* and *ageing SD* simulations in open black and filled red symbols, respectively. Uncertainties are defined as the error on the mean of the distribution in each energy bin. It can be clearly seen that there is a difference between the two simulation modes, with a worse resolution in the case of ageing SD. To quantify this difference, the resolution due to the ageing ($\sigma_E^{\rm ageing}$) is obtained as the quadratic difference between the resolution of the two modes, as follows:

$$\sigma_E^{\rm ageing} = \sqrt{(\sigma_E^{\rm ageingSD})^2 - (\sigma_E^{\rm ideal})^2} \tag{3}$$

In Fig. 4, right bottom panel, the evolution of $\sigma_E^{\rm ageing}$ is shown. The lower the energy, the worse the resolution, which is $\approx 4\%$ for 3 EeV and reaches 2% for the highest energies. The same behavior has been observed for heavier nuclei, with values between 2 and 4%.

The effect of the ageing has been observed in high-level analyses that use station signal information such as the risetime. This observable represents the time needed for the integrated signal to rise from 10% to 50% of its total value and thus is dependent on the value of τ. The risetimes

of the signals recorded in stations of an event are related to the muon content of the shower. This property has been used to infer the primary mass event-by-event with the "Δ method" [11]. This method combines the risetime information of all the stations triggered during an event into a single parameter called Δ, defined as follows:

$$\langle\Delta\rangle = \frac{1}{N}\sum_{i=1}^{N}\Delta_i = \frac{1}{N}\sum_{i=1}^{N}\frac{t_{1/2} - t_{1/2}^{bench}}{\sigma_{1/2}} \quad (4)$$

where $\langle\Delta\rangle$ is the average of Δ_i, which is defined as the deviation of the individual risetimes ($t_{1/2}$) of an event from a specific benchmark weighted by their uncertainty $\sigma_{1/2}$, and N is the number of triggered WCDs in the event. Simulated events are selected with the same criteria described in [11], and the $\langle\Delta\rangle$ method is performed on simulations. Due to the muon deficit in simulations with respect to data [12], to compare them, a normalization to the mean is performed. The result, illustrated in Fig. 5, shows that simulations that include the surface detector's evolution can reproduce the $\langle\Delta\rangle$ evolution over time observed in data. This decrease of $\langle\Delta\rangle$ over time is ≈ 0.2, over the full range of $\langle\Delta\rangle$ that spans between [-2,2] for different primaries and different energies.

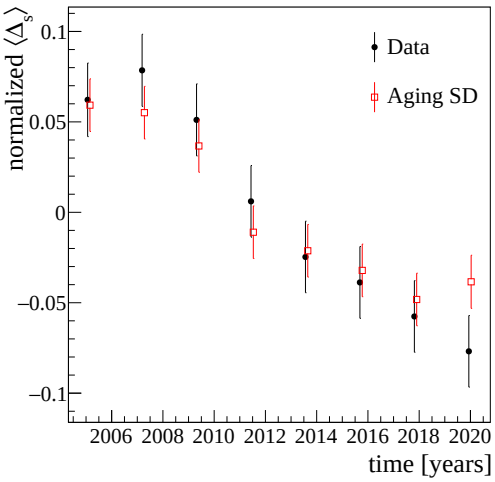

Figure 5: $\langle\Delta\rangle$ evolution over the years: data in black, simulations including ageing in red.

3. Improving the calibration: coincidence histograms

As shown previously, one of the effects of ageing is the increased attenuation of light in WCDs, which causes the atmospheric muon hump to merge into the electromagnetic background, making it more difficult to determine the charge corresponding to 1 VEM accurately. This difficulty can be mitigated by requiring a coincidence between the SSD and WCD, reducing the electromagnetic contribution. The new principle for building the calibration histograms is based on a 2-fold condition: when the signal in the WCD meets a certain threshold, a peak signal of more than 10 FADC counts is searched for in the SSD in a time window of 420 ns relative to the trigger. The method allows us to enhance the peak in the calibration histograms for aged stations, as shown in Fig. 6 for the station Owen. The merging of the muon peak in the e.m. background might bias the calibration constants; a correlation between the bias of the muon peak position (between the standard calibration and the coincidence calibration) and valley-to-hump ratio v/h (the measure of how severely the muon peak merges into the electromagnetic background in the standard calibration) is currently being investigated. Another advantage of the coincidence calibration histograms is that for the first time, a reliable estimate of the muon hump in the peak histograms, for which the muon hump was difficult to resolve, will be possible. This will improve the resolution in the normalization of measured traces when calibrating in units of VEM peak for the next studies utilizing the time distributions of the particles reaching the ground.

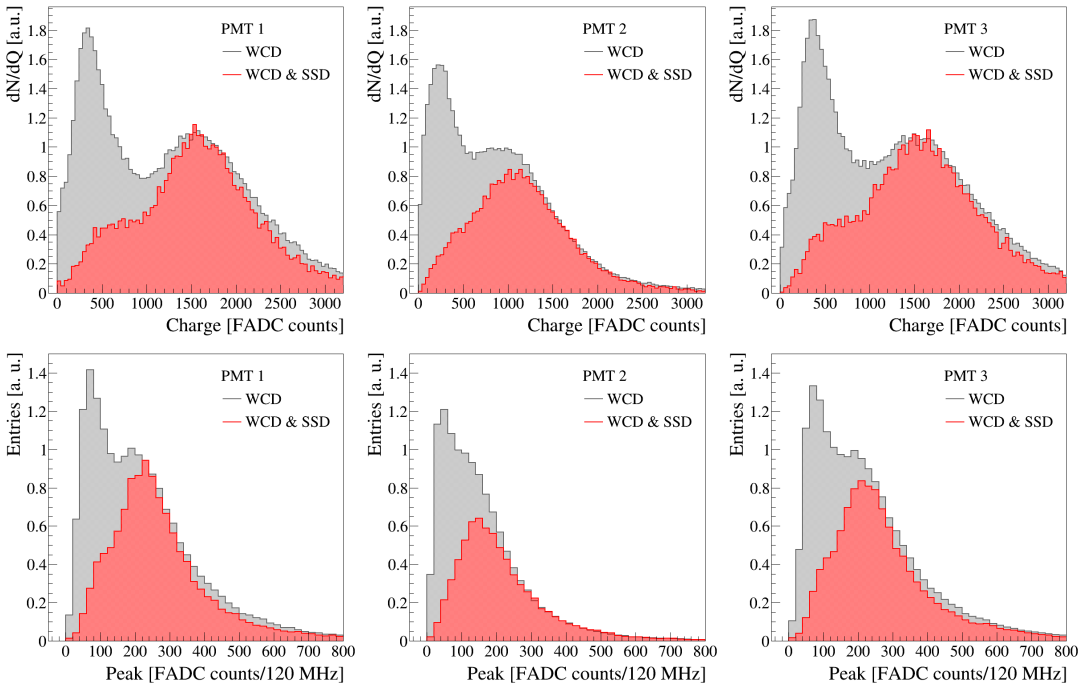

Figure 6: Examples of calibration histograms, charge (top) and peak (bottom), for station Owen in 2022. Red histograms are obtained requiring a coincidence between WCDs and SSDs.

4. Conclusions

To address and describe the observed ageing of the SD, detailed time-dependent simulations of the SD have been implemented and show that the energy reconstruction is unbiased by ageing, while the energy resolution has worsened by about 5%. The use of more realistic simulations of the SD response will improve the current and future systematic uncertainties in the interpretation of measurements while enhancing the potential of deep-learning algorithms, which require a very good matching between measurement and simulations. At the same time, the WCD-SSD coincidence calibration method will guarantee a high-accuracy calibration of the water Cherenkov detectors for at least another 15 years of operation, irrespective of the further ageing of its components.

References

[1] A. Aab *et al.* [Pierre Auger coll.], JINST **15** (2020) P10021.
[2] X. Bertou *et al.* [Pierre Auger coll.], NIM A **568** (2006) 839-846.
[3] A. Aab *et al.* [Pierre Auger coll.], JINST **15** (2020) P09002.
[4] A. Castellina *et al.* [Pierre Auger coll.], EPJ Web Conf. **210** (2019) 06002 [1905.04472].
[5] K. Choi *et al.* [Pierre Auger Coll.], PoS(ICRC2019) **222** (2019).
[6] S. Argirò *et al.*, NIM A **580** (2007) 1485-1496.
[7] J. Abraham *et al.* [Pierre Auger Coll.], NIM A **613** (2010) 29-39.
[8] D. Heck *et al.*, Report FZKA **60119** (1998) .
[9] Pierog, T. *et al.* [Pierre Auger Coll.], Phys. Rev. C **92** (2015) 034906.
[10] A. Aab *et al.* [Pierre Auger Coll.], Phys. Rev. D **102** (2020) 062005.
[11] C. J. Todero Peixoto *et al.* [Pierre Auger Coll.], PoS(ICRC2019) **440** (2019)
[12] A. Aab *et al.* [Pierre Auger Coll.], EPJ C **80** (2020) 751.

The Pierre Auger Collaboration

A. Abdul Halim[13], P. Abreu[72], M. Aglietta[54,52], I. Allekotte[1], K. Almeida Cheminant[70], A. Almela[7,12], R. Aloisio[45,46], J. Alvarez-Muñiz[79], J. Ammerman Yebra[79], G.A. Anastasi[54,52], L. Anchordoqui[86], B. Andrada[7], S. Andringa[72], C. Aramo[50], P.R. Araújo Ferreira[42], E. Arnone[63,52], J. C. Arteaga Velázquez[67], H. Asorey[7], P. Assis[72], G. Avila[11], E. Avocone[57,46], A.M. Badescu[75], A. Bakalova[32], A. Balaceanu[73], F. Barbato[45,46], A. Bartz Mocellin[85], J.A. Bellido[13,69], C. Berat[36], M.E. Bertaina[63,52], G. Bhatta[70], M. Bianciotto[63,52], P.L. Biermann[h], V. Binet[5], K. Bismark[39,7], T. Bister[80,81], J. Biteau[37], J. Blazek[32], C. Bleve[36], J. Blümer[41], M. Boháčová[32], D. Boncioli[57,46], C. Bonifazi[8,26], L. Bonneau Arbeletche[21], N. Borodai[70], J. Brack[j], P.G. Brichetto Orchera[7], F.L. Briechle[42], A. Bueno[78], S. Buitink[15], M. Buscemi[47,61], M. Büsken[39,7], A. Bwembya[80,81], K.S. Caballero-Mora[66], S. Cabana-Freire[79], L. Caccianiga[59,49], I. Caracas[38], R. Caruso[58,47], A. Castellina[54,52], F. Catalani[18], G. Cataldi[48], L. Cazon[79], M. Cerda[10], A. Cermenati[45,46], J.A. Chinellato[21], J. Chudoba[32], L. Chytka[33], R.W. Clay[13], A.C. Cobos Cerutti[6], R. Colalillo[60,50], A. Coleman[90], M.R. Coluccia[48], R. Conceição[72], A. Condorelli[37], G. Consolati[49,55], M. Conte[56,48], F. Convenga[41], D. Correia dos Santos[28], P.J. Costa[72], C.E. Covault[84], M. Cristinziani[44], C.S. Cruz Sanchez[3], S. Dasso[4,2], K. Daumiller[41], B.R. Dawson[13], R.M. de Almeida[28], J. de Jesús[7,41], S.J. de Jong[80,81], J.R.T. de Mello Neto[26,27], I. De Mitri[45,46], J. de Oliveira[17], D. de Oliveira Franco[21], F. de Palma[56,48], V. de Souza[19], E. De Vito[56,48], A. Del Popolo[58,47], O. Deligny[34], N. Denner[32], L. Deval[41,7], A. di Matteo[52], M. Dobre[73], C. Dobrigkeit[21], J.C. D'Olivo[68], L.M. Domingues Mendes[72], J.C. dos Anjos, R.C. dos Anjos[25], J. Ebr[32], F. Ellwanger[41], M. Emam[80,81], R. Engel[39,41], I. Epicoco[56,48], M. Erdmann[42], A. Etchegoyen[7,12], C. Evoli[45,46], H. Falcke[80,82,81], J. Farmer[89], G. Farrar[88], A.C. Fauth[21], N. Fazzini[e], F. Feldbusch[40], F. Fenu[41,d], A. Fernandes[72], B. Fick[87], J.M. Figueira[7], A. Filipčič[77,76], T. Fitoussi[41], B. Flaggs[90], T. Fodran[80], T. Fujii[89,f], A. Fuster[7,12], C. Galea[80], C. Galelli[59,49], B. García[6], C. Gaudu[38], H. Gemmeke[40], F. Gesualdi[7,41], A. Gherghel-Lascu[73], P.L. Ghia[34], U. Giaccari[48], M. Giammarchi[49], J. Glombitza[42,g], F. Gobbi[10], F. Gollan[7], G. Golup[1], M. Gómez Berisso[1], P.F. Gómez Vitale[11], J.P. Gongora[11], J.M. González[1], N. González[7], I. Goos[1], D. Góra[70], A. Gorgi[54,52], M. Gottowik[79], T.D. Grubb[13], F. Guarino[60,50], G.P. Guedes[22], E. Guido[44], S. Hahn[39], P. Hamal[32], M.R. Hampel[7], P. Hansen[3], D. Harari[1], V.M. Harvey[13], A. Haungs[41], T. Hebbeker[42], C. Hojvat[e], J.R. Hörandel[80,81], P. Horvath[33], M. Hrabovský[33], T. Huege[41,15], A. Insolia[58,47], P.G. Isar[74], P. Janecek[32], J.A. Johnsen[85], J. Jurysek[32], A. Kääpä[38], K.H. Kampert[38], B. Keilhauer[41], A. Khakurdikar[80], V.V. Kizakke Covilakam[7,41], H.O. Klages[41], M. Kleifges[40], F. Knapp[39], N. Kunka[40], B.L. Lago[16], N. Langner[42], M.A. Leigui de Oliveira[24], Y Lema-Capeans[79], V. Lenok[39], A. Letessier-Selvon[35], I. Lhenry-Yvon[34], D. Lo Presti[58,47], L. Lopes[72], L. Lu[91], Q. Luce[39], J.P. Lundquist[76], A. Machado Payeras[21], M. Majercakova[32], D. Mandat[32], B.C. Manning[13], P. Mantsch[e], S. Marafico[34], F.M. Mariani[59,49], A.G. Mariazzi[3], I.C. Mariş[14], G. Marsella[61,47], D. Martello[56,48], S. Martinelli[41,7], O. Martínez Bravo[64], M.A. Martins[79], M. Mastrodicasa[57,46], H.J. Mathes[41], J. Matthews[a], G. Matthiae[62,51], E. Mayotte[85,38], S. Mayotte[85], P.O. Mazur[e], G. Medina-Tanco[68], J. Meinert[38], D. Melo[7], A. Menshikov[40], C. Merx[41], S. Michal[33], M.I. Micheletti[5], L. Miramonti[59,49], S. Mollerach[1], F. Montanet[36], L. Morejon[38], C. Morello[54,52], A.L. Müller[32], K. Mulrey[80,81], R. Mussa[52], M. Muzio[88], W.M. Namasaka[38], S. Negi[32], L. Nellen[68], K. Nguyen[87], G. Nicora[9], M. Niculescu-Oglinzanu[73], M. Niechciol[44], D. Nitz[87], D. Nosek[31], V. Novotny[31], L. Nožka[33], A Nucita[56,48], L.A. Núñez[30], C. Oliveira[19], M. Palatka[32], J. Pallotta[9], S. Panja[32], G. Parente[79], T. Paulsen[38], J. Pawlowsky[38], M. Pech[32], J. Pękala[70], R. Pelayo[65], L.A.S. Pereira[23], E.E. Pereira Martins[39,7], J. Perez Armand[20], C. Pérez Bertolli[7,41], L. Perrone[56,48], S. Petrera[45,46], C. Petrucci[57,46], T. Pierog[41], M. Pimenta[72], M. Platino[7], B. Pont[80], M. Pothast[81,80], M. Pourmohammad Shahvar[61,47], P. Privitera[89], M. Prouza[32], A. Puyleart[87], S. Querchfeld[38], J. Rautenberg[38], D. Ravignani[7], M. Reininghaus[39], J. Ridky[32], F. Riehn[79], M. Risse[44], V. Rizi[57,46], W. Rodrigues de Carvalho[80], E. Rodriguez[7,41], J. Rodriguez Rojo[11], M.J. Roncoroni[7], S. Rossoni[43], M. Roth[41], E. Roulet[1], A.C. Rovero[4], P. Ruehl[44], A. Saftoiu[73], M. Saharan[80], F. Salamida[57,46], H. Salazar[64], G. Salina[51], J.D. Sanabria Gomez[30], F. Sánchez[7], E.M. Santos[20], E. Santos[32],

F. Sarazin[85], R. Sarmento[72], R. Sato[11], P. Savina[91], C.M. Schäfer[41], V. Scherini[56,48], H. Schieler[41], M. Schimassek[34], M. Schimp[38], F. Schlüter[41], D. Schmidt[39], O. Scholten[15,i], H. Schoorlemmer[80,81], P. Schovánek[32], F.G. Schröder[90,41], J. Schulte[42], T. Schulz[41], S.J. Sciutto[3], M. Scornavacche[7,41], A. Segreto[53,47], S. Sehgal[38], S.U. Shivashankara[76], G. Sigl[43], G. Silli[7], O. Sima[73,b], F. Simon[40], R. Smau[73], R. Šmída[89], P. Sommers[k], J.F. Soriano[86], R. Squartini[10], M. Stadelmaier[32], D. Stanca[73], S. Stanič[76], J. Stasielak[70], P. Stassi[36], S. Strähnz[39], M. Straub[42], M. Suárez-Durán[14], T. Suomijärvi[37], A.D. Supanitsky[7], Z. Svozilikova[32], Z. Szadkowski[71], A. Tapia[29], C. Taricco[63,52], C. Timmermans[81,80], O. Tkachenko[41], P. Tobiska[32], C.J. Todero Peixoto[18], B. Tomé[72], Z. Torrès[36], A. Travaini[10], P. Travnicek[32], C. Trimarelli[57,46], M. Tueros[3], M. Unger[41], L. Vaclavek[33], M. Vacula[33], J.F. Valdés Galicia[68], L. Valore[60,50], E. Varela[64], A. Vásquez-Ramírez[30], D. Veberič[41], C. Ventura[27], I.D. Vergara Quispe[3], V. Verzi[51], J. Vicha[32], J. Vink[83], J. Vlastimil[32], S. Vorobiov[76], C. Watanabe[26], A.A. Watson[c], A. Weindl[41], L. Wiencke[85], H. Wilczyński[70], D. Wittkowski[38], B. Wundheiler[7], B. Yue[38], A. Yushkov[32], O. Zapparrata[14], E. Zas[79], D. Zavrtanik[76,77], M. Zavrtanik[77,76]

———— • ————

[1] Centro Atómico Bariloche and Instituto Balseiro (CNEA-UNCuyo-CONICET), San Carlos de Bariloche, Argentina
[2] Departamento de Física and Departamento de Ciencias de la Atmósfera y los Océanos, FCEyN, Universidad de Buenos Aires and CONICET, Buenos Aires, Argentina
[3] IFLP, Universidad Nacional de La Plata and CONICET, La Plata, Argentina
[4] Instituto de Astronomía y Física del Espacio (IAFE, CONICET-UBA), Buenos Aires, Argentina
[5] Instituto de Física de Rosario (IFIR) – CONICET/U.N.R. and Facultad de Ciencias Bioquímicas y Farmacéuticas U.N.R., Rosario, Argentina
[6] Instituto de Tecnologías en Detección y Astropartículas (CNEA, CONICET, UNSAM), and Universidad Tecnológica Nacional – Facultad Regional Mendoza (CONICET/CNEA), Mendoza, Argentina
[7] Instituto de Tecnologías en Detección y Astropartículas (CNEA, CONICET, UNSAM), Buenos Aires, Argentina
[8] International Center of Advanced Studies and Instituto de Ciencias Físicas, ECyT-UNSAM and CONICET, Campus Miguelete – San Martín, Buenos Aires, Argentina
[9] Laboratorio Atmósfera – Departamento de Investigaciones en Láseres y sus Aplicaciones – UNIDEF (CITEDEF-CONICET), Argentina
[10] Observatorio Pierre Auger, Malargüe, Argentina
[11] Observatorio Pierre Auger and Comisión Nacional de Energía Atómica, Malargüe, Argentina
[12] Universidad Tecnológica Nacional – Facultad Regional Buenos Aires, Buenos Aires, Argentina
[13] University of Adelaide, Adelaide, S.A., Australia
[14] Université Libre de Bruxelles (ULB), Brussels, Belgium
[15] Vrije Universiteit Brussels, Brussels, Belgium
[16] Centro Federal de Educação Tecnológica Celso Suckow da Fonseca, Petropolis, Brazil
[17] Instituto Federal de Educação, Ciência e Tecnologia do Rio de Janeiro (IFRJ), Brazil
[18] Universidade de São Paulo, Escola de Engenharia de Lorena, Lorena, SP, Brazil
[19] Universidade de São Paulo, Instituto de Física de São Carlos, São Carlos, SP, Brazil
[20] Universidade de São Paulo, Instituto de Física, São Paulo, SP, Brazil
[21] Universidade Estadual de Campinas, IFGW, Campinas, SP, Brazil
[22] Universidade Estadual de Feira de Santana, Feira de Santana, Brazil
[23] Universidade Federal de Campina Grande, Centro de Ciencias e Tecnologia, Campina Grande, Brazil
[24] Universidade Federal do ABC, Santo André, SP, Brazil
[25] Universidade Federal do Paraná, Setor Palotina, Palotina, Brazil
[26] Universidade Federal do Rio de Janeiro, Instituto de Física, Rio de Janeiro, RJ, Brazil
[27] Universidade Federal do Rio de Janeiro (UFRJ), Observatório do Valongo, Rio de Janeiro, RJ, Brazil
[28] Universidade Federal Fluminense, EEIMVR, Volta Redonda, RJ, Brazil
[29] Universidad de Medellín, Medellín, Colombia
[30] Universidad Industrial de Santander, Bucaramanga, Colombia

[31] Charles University, Faculty of Mathematics and Physics, Institute of Particle and Nuclear Physics, Prague, Czech Republic
[32] Institute of Physics of the Czech Academy of Sciences, Prague, Czech Republic
[33] Palacky University, Olomouc, Czech Republic
[34] CNRS/IN2P3, IJCLab, Université Paris-Saclay, Orsay, France
[35] Laboratoire de Physique Nucléaire et de Hautes Energies (LPNHE), Sorbonne Université, Université de Paris, CNRS-IN2P3, Paris, France
[36] Univ. Grenoble Alpes, CNRS, Grenoble Institute of Engineering Univ. Grenoble Alpes, LPSC-IN2P3, 38000 Grenoble, France
[37] Université Paris-Saclay, CNRS/IN2P3, IJCLab, Orsay, France
[38] Bergische Universität Wuppertal, Department of Physics, Wuppertal, Germany
[39] Karlsruhe Institute of Technology (KIT), Institute for Experimental Particle Physics, Karlsruhe, Germany
[40] Karlsruhe Institute of Technology (KIT), Institut für Prozessdatenverarbeitung und Elektronik, Karlsruhe, Germany
[41] Karlsruhe Institute of Technology (KIT), Institute for Astroparticle Physics, Karlsruhe, Germany
[42] RWTH Aachen University, III. Physikalisches Institut A, Aachen, Germany
[43] Universität Hamburg, II. Institut für Theoretische Physik, Hamburg, Germany
[44] Universität Siegen, Department Physik – Experimentelle Teilchenphysik, Siegen, Germany
[45] Gran Sasso Science Institute, L'Aquila, Italy
[46] INFN Laboratori Nazionali del Gran Sasso, Assergi (L'Aquila), Italy
[47] INFN, Sezione di Catania, Catania, Italy
[48] INFN, Sezione di Lecce, Lecce, Italy
[49] INFN, Sezione di Milano, Milano, Italy
[50] INFN, Sezione di Napoli, Napoli, Italy
[51] INFN, Sezione di Roma "Tor Vergata", Roma, Italy
[52] INFN, Sezione di Torino, Torino, Italy
[53] Istituto di Astrofisica Spaziale e Fisica Cosmica di Palermo (INAF), Palermo, Italy
[54] Osservatorio Astrofisico di Torino (INAF), Torino, Italy
[55] Politecnico di Milano, Dipartimento di Scienze e Tecnologie Aerospaziali , Milano, Italy
[56] Università del Salento, Dipartimento di Matematica e Fisica "E. De Giorgi", Lecce, Italy
[57] Università dell'Aquila, Dipartimento di Scienze Fisiche e Chimiche, L'Aquila, Italy
[58] Università di Catania, Dipartimento di Fisica e Astronomia "Ettore Majorana", Catania, Italy
[59] Università di Milano, Dipartimento di Fisica, Milano, Italy
[60] Università di Napoli "Federico II", Dipartimento di Fisica "Ettore Pancini", Napoli, Italy
[61] Università di Palermo, Dipartimento di Fisica e Chimica "E. Segrè", Palermo, Italy
[62] Università di Roma "Tor Vergata", Dipartimento di Fisica, Roma, Italy
[63] Università Torino, Dipartimento di Fisica, Torino, Italy
[64] Benemérita Universidad Autónoma de Puebla, Puebla, México
[65] Unidad Profesional Interdisciplinaria en Ingeniería y Tecnologías Avanzadas del Instituto Politécnico Nacional (UPIITA-IPN), México, D.F., México
[66] Universidad Autónoma de Chiapas, Tuxtla Gutiérrez, Chiapas, México
[67] Universidad Michoacana de San Nicolás de Hidalgo, Morelia, Michoacán, México
[68] Universidad Nacional Autónoma de México, México, D.F., México
[69] Universidad Nacional de San Agustin de Arequipa, Facultad de Ciencias Naturales y Formales, Arequipa, Peru
[70] Institute of Nuclear Physics PAN, Krakow, Poland
[71] University of Łódź, Faculty of High-Energy Astrophysics,Łódź, Poland
[72] Laboratório de Instrumentação e Física Experimental de Partículas – LIP and Instituto Superior Técnico – IST, Universidade de Lisboa – UL, Lisboa, Portugal
[73] "Horia Hulubei" National Institute for Physics and Nuclear Engineering, Bucharest-Magurele, Romania
[74] Institute of Space Science, Bucharest-Magurele, Romania
[75] University Politehnica of Bucharest, Bucharest, Romania
[76] Center for Astrophysics and Cosmology (CAC), University of Nova Gorica, Nova Gorica, Slovenia
[77] Experimental Particle Physics Department, J. Stefan Institute, Ljubljana, Slovenia

PoS(ICRC2023)266

[78] Universidad de Granada and C.A.F.P.E., Granada, Spain
[79] Instituto Galego de Física de Altas Enerxías (IGFAE), Universidade de Santiago de Compostela, Santiago de Compostela, Spain
[80] IMAPP, Radboud University Nijmegen, Nijmegen, The Netherlands
[81] Nationaal Instituut voor Kernfysica en Hoge Energie Fysica (NIKHEF), Science Park, Amsterdam, The Netherlands
[82] Stichting Astronomisch Onderzoek in Nederland (ASTRON), Dwingeloo, The Netherlands
[83] Universiteit van Amsterdam, Faculty of Science, Amsterdam, The Netherlands
[84] Case Western Reserve University, Cleveland, OH, USA
[85] Colorado School of Mines, Golden, CO, USA
[86] Department of Physics and Astronomy, Lehman College, City University of New York, Bronx, NY, USA
[87] Michigan Technological University, Houghton, MI, USA
[88] New York University, New York, NY, USA
[89] University of Chicago, Enrico Fermi Institute, Chicago, IL, USA
[90] University of Delaware, Department of Physics and Astronomy, Bartol Research Institute, Newark, DE, USA
[91] University of Wisconsin-Madison, Department of Physics and WIPAC, Madison, WI, USA

—

[a] Louisiana State University, Baton Rouge, LA, USA
[b] also at University of Bucharest, Physics Department, Bucharest, Romania
[c] School of Physics and Astronomy, University of Leeds, Leeds, United Kingdom
[d] now at Agenzia Spaziale Italiana (ASI). Via del Politecnico 00133, Roma, Italy
[e] Fermi National Accelerator Laboratory, Fermilab, Batavia, IL, USA
[f] now at Graduate School of Science, Osaka Metropolitan University, Osaka, Japan
[g] now at ECAP, Erlangen, Germany
[h] Max-Planck-Institut für Radioastronomie, Bonn, Germany
[i] also at Kapteyn Institute, University of Groningen, Groningen, The Netherlands
[j] Colorado State University, Fort Collins, CO, USA
[k] Pennsylvania State University, University Park, PA, USA

Acknowledgments

The successful installation, commissioning, and operation of the Pierre Auger Observatory would not have been possible without the strong commitment and effort from the technical and administrative staff in Malargüe. We are very grateful to the following agencies and organizations for financial support:

Argentina – Comisión Nacional de Energía Atómica; Agencia Nacional de Promoción Científica y Tecnológica (ANPCyT); Consejo Nacional de Investigaciones Científicas y Técnicas (CONICET); Gobierno de la Provincia de Mendoza; Municipalidad de Malargüe; NDM Holdings and Valle Las Leñas; in gratitude for their continuing cooperation over land access; Australia – the Australian Research Council; Belgium – Fonds de la Recherche Scientifique (FNRS); Research Foundation Flanders (FWO); Brazil – Conselho Nacional de Desenvolvimento Científico e Tecnológico (CNPq); Financiadora de Estudos e Projetos (FINEP); Fundação de Amparo à Pesquisa do Estado de Rio de Janeiro (FAPERJ); São Paulo Research Foundation (FAPESP) Grants No. 2019/10151-2, No. 2010/07359-6 and No. 1999/05404-3; Ministério da Ciência, Tecnologia, Inovações e Comunicações (MCTIC); Czech Republic – Grant No. MSMT CR LTT18004, LM2015038, LM2018102, CZ.02.1.01/0.0/0.0/16_013/0001402, CZ.02.1.01/0.0/0.0/18_046/0016010 and CZ.02.1.01/0.0/0.0/17_049/0008422; France – Centre de Calcul IN2P3/CNRS; Centre National de la Recherche Scientifique (CNRS); Conseil Régional Ile-de-France; Département Physique Nucléaire et Corpusculaire (PNC-IN2P3/CNRS); Département Sciences de l'Univers (SDU-INSU/CNRS); Institut Lagrange de Paris (ILP) Grant No. LABEX ANR-10-LABX-63 within the Investissements d'Avenir Programme Grant No. ANR-11-IDEX-0004-02; Germany – Bundesministerium für Bildung und Forschung (BMBF); Deutsche Forschungsgemeinschaft (DFG); Finanzministerium Baden-Württemberg; Helmholtz Alliance for Astroparticle Physics (HAP); Helmholtz-Gemeinschaft Deutscher Forschungszentren (HGF); Ministerium für Kultur und Wissenschaft des Landes Nordrhein-Westfalen; Ministerium für Wissenschaft, Forschung und Kunst des Landes Baden-Württemberg; Italy – Istituto Nazionale di Fisica Nucleare (INFN); Istituto Nazionale di Astrofisica (INAF); Ministero dell'Universitá e della Ricerca (MUR); CETEMPS Center of Excellence; Ministero degli Affari Esteri (MAE), ICSC Centro Nazionale di Ricerca in High Performance Computing, Big Data

and Quantum Computing, funded by European Union NextGenerationEU, reference code CN_00000013; México – Consejo Nacional de Ciencia y Tecnología (CONACYT) No. 167733; Universidad Nacional Autónoma de México (UNAM); PAPIIT DGAPA-UNAM; The Netherlands – Ministry of Education, Culture and Science; Netherlands Organisation for Scientific Research (NWO); Dutch national e-infrastructure with the support of SURF Cooperative; Poland – Ministry of Education and Science, grants No. DIR/WK/2018/11 and 2022/WK/12; National Science Centre, grants No. 2016/22/M/ST9/00198, 2016/23/B/ST9/01635, 2020/39/B/ST9/01398, and 2022/45/B/ST9/02163; Portugal – Portuguese national funds and FEDER funds within Programa Operacional Factores de Competitividade through Fundação para a Ciência e a Tecnologia (COMPETE); Romania – Ministry of Research, Innovation and Digitization, CNCS-UEFISCDI, contract no. 30N/2023 under Romanian National Core Program LAPLAS VII, grant no. PN 23 21 01 02 and project number PN-III-P1-1.1-TE-2021-0924/TE57/2022, within PNCDI III; Slovenia – Slovenian Research Agency, grants P1-0031, P1-0385, I0-0033, N1-0111; Spain – Ministerio de Economía, Industria y Competitividad (FPA2017-85114-P and PID2019-104676GB-C32), Xunta de Galicia (ED431C 2017/07), Junta de Andalucía (SOMM17/6104/UGR, P18-FR-4314) Feder Funds, RENATA Red Nacional Temática de Astropartículas (FPA2015-68783-REDT) and María de Maeztu Unit of Excellence (MDM-2016-0692); USA – Department of Energy, Contracts No. DE-AC02-07CH11359, No. DE-FR02-04ER41300, No. DE-FG02-99ER41107 and No. DE-SC0011689; National Science Foundation, Grant No. 0450696; The Grainger Foundation; Marie Curie-IRSES/EPLANET; European Particle Physics Latin American Network; and UNESCO.